LOAD CAPACITY OF COLD-FORMED Z-SECTIONS

P. TOMKA

Department of Steel Structures,
Technical University, H-1521 Budapest

Received October 5, 1984
Presented by Prof. Dr. Ottó Halász

Abstract

Calculation of cold-formed *Z*-beams supported by sheeting according to the second-order theory has been presented. Theoretical results are confronted to test results for purlins under wind suction. The outlined method suits spatial model design of beams where the effect of residual stresses is reckoned with as fictitious inaccuracies.

Introduction

A high percentage of structural members (purlins, side-rails) directly supporting the sheeting of steel-structure halls are made of cold-formed sections, actualizing economical though safe design. Theoretical-experimental analysis of purlins made of cold-formed *Z*-sections will be considered, involving a structural design where top flange of the beam is continuously supported by the sheeting, preventing at the same time

— displacement of the supported flange in the plane of sheeting; and

— relative rotation of sheeting and flange.

The sheeting-beam joint also suits to take torque. A detailed analysis will be spent on simply supported beams exposed to wind suction, a load type likely to be critical for partly open halls, while the design cannot be considered as fully solved for *Z*-sections.

The actual design practice

Design specifications for cold-formed, thin-walled sections are found in [5]. Its calculation methods relying on first-order theory, involving approximations, have been shown in our tests not to truly reflect the actual behaviour of *Z*-section beams, even may lead to structural underdimensioning, arguing for a more exact analysis, taking also secondary effects into consideration.

Second-order approximation

Typical cross sections of the tested beam are seen in Fig. 1. Beam cross sections at supports are seen in Fig. 1.a, while an intermediate cross section of the unloaded beam is seen in Fig. 1.b. Initial imperfections (φ_0, u_0) vary along the beam length.

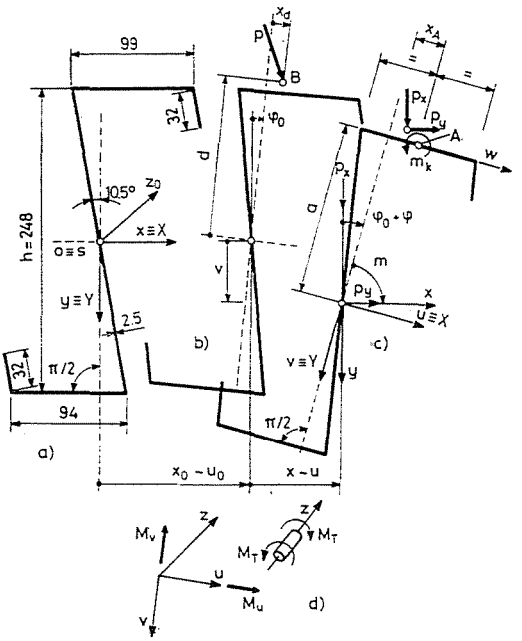

Fig. 1

Position of, and forces acting on, the beam mid-section after deformation have been plotted in Fig. 1.c. Load p with point of application B keeps its direction after deformation.

The section is assumed to rotate around restrained axis A. The section is practically point symmetrical hence centroid and shear centre coincide.

Forces reduced to the shear centre are:

$$m = -p_x[(\varphi_0 + \varphi)d + x_d] - p_y d - wa + m_k$$

Considering that, although the cross section is point symmetrical but neither X nor Y are its symmetry axes, equilibrium of bending moments becomes:

$$-EJ_y u'' - EJ_{xy} v'' = M_v \tag{1}$$

$$-EJ_{xy} u'' - EJ_x v'' = M_u \tag{2}$$

From (2):

$$v'' = -\frac{M_u + EJ_{xy} u''}{EJ_x} \tag{3}$$

substituted into (1):

$$-E\left[J_y - \frac{J_{xy}^2}{J_x}\right] u'' + \frac{J_{xy}}{J_x} M_u = M_v \tag{4}$$

Taking also rotation $\varphi_0 + \varphi$ of the cross section into consideration:

$$M_v = M_{w,p} + (\varphi_0 + \varphi) M_{px}$$

Bending moment $M_{w,p}$ arises from component of load p along u, and from distributed reaction force w due to the supporting effect of the sheeting. Hence:

$$-E\tilde{J}_y u'' + \frac{J_{xy}}{J_x} M_{px} - M_{w,p} - (\varphi_0 + \varphi) M_{px} = 0$$

derived twice with respect to z and substituting

$$M'_{px} = T_x$$
$$M''_{px} = -p_x$$
$$M''_{w,p} = -w - p_y$$

to yield the distributed reaction force:

$$w = E\tilde{J}_y u^{IV} + M_{px}\varphi'' + 2T_x\varphi' - p_x\varphi + \\ + \frac{J_{xy}}{J_x} p_x - p_y + M_{px}\varphi''_0 + 2T_x\varphi'_0 - p_x\varphi_0 \qquad (5)$$

Torque of the cross section with coordinate z due to external forces has three parts:

a) Cross section gets into position

$$u_0 + u; \quad v$$

hence:

$$M_{T_1} = (u_0 + u)' M_{px} - v' M_v$$

b) Torque due to (generatrix) rotation:

$$M_{T_2} = -(\varphi_0 + \varphi)' \int_{(A)} \sigma r^2 \, dA$$

c) Torque from forces parallel to plane y—z_0 (see Fig. 2):

$$M_{T_3} = M_{T_3(z=0)} - R_x[u_{0(z)} + u_{(z)}] + p_x \int_0^z \{[u_{0(z)} + u_{(z)}] - [u_{0(\zeta)} + u_{(\zeta)}]\} d\zeta$$

Since

$$R_x - p_x z = T_x$$

$$M_{T_3} = M_{T_3(z=0)} - T_x[u_{0(z)} + u_{(z)}] - p_x \int_0^z [u_{0(\zeta)} + u_{(\zeta)}] \, d\zeta$$

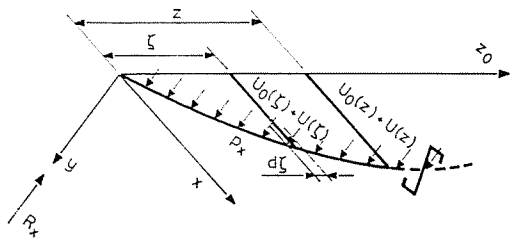

Fig. 2

Equilibrium of external and internal torques derived one times with respect to z yields the distributed torque:

$$(GJ_{cs}\,\varphi' - EJ_\omega\varphi''')' - (M_{T_1} + M_{T_2} + M_{T_3})' = m$$

that is:

$$EJ_\omega\varphi^{IV} - GJ_{cs}\varphi'' + (u_0 + u)''M_{px} + (u_0 + u)'\,T_x - (v'\,M_v) -$$
$$- [(\varphi_0 + \varphi)' \int_{(A)} \sigma r^2\,dA]' - T_x'(u_0 + u) - T_x(u_0 + u)' - p_x(u_0 + u) -$$
$$- p_x[(\varphi_0 + \varphi)\,d + x_d] - p_y d - wa + m_k = 0$$

The section is rotated around restrained axis A, and top flange displacement along u is zero, hence, for the shear centre:

$$u = -\sqrt{a^2 + x_A^2}\;\varphi \sim -a\varphi$$

Furthermore:

$$(\varphi_0 + \varphi)' \int_{(A)} \sigma r^2\,dA \sim 0$$

because of the point symmetry of the section; higher powers of rotations are neglected, and so is the effect of torque $v'Mv$.

Substituting values

$$m_k = k\varphi$$
$$d \sim a \sim h/2$$

and Eq. (5) yields:

$$E\bar{J}_\omega\varphi^{IV} - \varphi''(2aM_{px} + GJ_{cs}) - 2aT_x\varphi' + \varphi k =$$
$$= p_x\left(a\frac{J_{xy}}{J_x} + x_d\right) + M_{px}(a\varphi_0'' - u_0'') + 2a\,T_x\varphi_0' - ap_x\,\varphi_0 \qquad (6)$$

where

$$\bar{J}_\omega = J_\omega + \left(\frac{h}{2}\right)^2\left(J_y - \frac{J_{xy}^2}{J_x}\right)$$

Right-hand side of this equation is non-zero even for beams without imperfections ($u_0 = \varphi_0 = 0$) and a load passing through the shear centre $x_d = 0$, of a value:

$$ap_x \frac{J_{xy}}{J_x}$$

and depends only on the load component parallel to plane $y—z_0$.

The point of application cannot be precisely given in general. In practical cases, with increasing load the point of application tends to the web and enhances rotations, as demonstrated by our tests.

Solution of differential equation (6) yields rotations φ of the beam cross section. Beam displacements along v are obtained by integrating twice Eq. (3).

Normal stresses in beam cross sections are calculated from bending and torsion.

Bending moments about axes X and Y of the rotated cross section are, respectively:

$$M_x = M_u \sim M_{px}$$

and, from Eq. (4):

$$M_y = M_v = E\bar{J}_\omega a\varphi'' + \frac{J_{xy}}{J_x} M_{px}$$

Bending stresses σ_x are obtained from the term for the cross section of general form:

$$\sigma_x = \frac{1}{D} [(J_{xy}X + J_y Y) M_x - (J_x X + J_{xy} Y) M_y]$$

Normal stresses due to torsion result from:

$$\sigma_\omega = E\bar{\omega}\varphi''$$

Distributed reaction force acting on purlin-sheeting connections and the structural member preventing sheeting displacements is obtained from [5].

Experimental

Recently, the Department of Steel Structures undertook a test series to find the load capacity of cold-formed Z-sections [1]. Test beams $F13$ and $F11$ were to test wind suction effect.

Theoretical results have been compared with values measured on both beams.

Test arrangement for the beam of span $L = 6$ m has been sketched in Fig. 3. The sheeting is made of corrugated aluminium sheet TR 65/180-0.8,

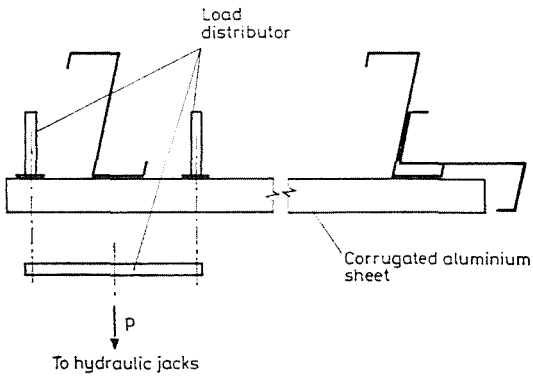

Fig. 3

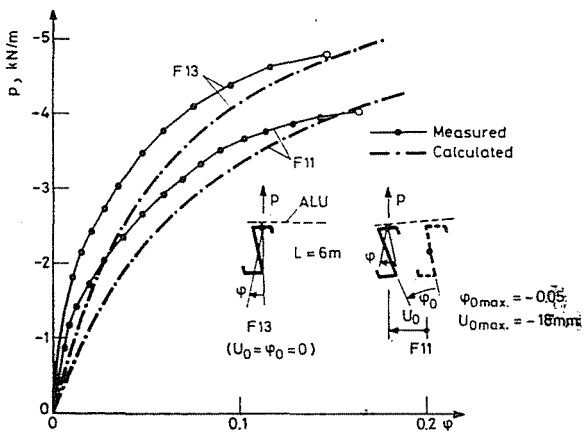

Fig. 4

fastened to the test beams using self-tapping screws in each valley. Stiffness of the right-side beam composed of two sections was sufficient to practically restrain top flanges of the tested beams from displacements parallel to the sheeting. Beam $F11$ has been mounted with initial imperfection, maximum initial rotation of the section being (at mid-beam):

$$\varphi_{0\max} = -0.05$$

and maximum shift of centroid along x:

$$x_{0\max} = -18 \text{ mm}.$$

Intermediate values of both initial imperfections are fairly approximated by a second-order parabola. Beam $F13$ had zero initial imperfection.

The distance x_d was assumed to be $+10$ mm. Value of coefficient k for the elastic restraining effect of the sheeting was assumed after [3] as 1.0 and 0.9 kN for beams $F13$ and $F11$, respectively.

Rotations of beam mid-sections are seen in Fig. 4. For low load values, actual rotations are much smaller. Namely — as stated before — application point of the load changes with increasing load, initially it is at the screws holding the sheeting (at mid-top-flange), to be shifted later toward the web. Irrespective of that, the calculated curve clearly points to the character of actual rotations, and near failure (circle-marked end point of measured curves) measured and calculated values little differ.

Normal stresses at beam mid-sections due to near-ultimate load have been plotted in Fig. 5. In connection with this diagram it should be noted that calculated stresses (in dash-and-dot line) with absolute values over

$$\sigma_F = 270 \text{ MPa}$$

(actual yield point) are in fact values proportional to the combination of strains.

From the diagram it is clear that high stresses arise at the flange to web junction — mainly on the compressed lower side — while the other edge of the compressed flange and the lip are practically unloaded. Calculated stresses, at least in the lower part inaffected by the direct effect of sheeting transferring the load, are rather close to this distribution.

Failure mode of both beams — as seen from load/rotation diagrams — was not lateral buckling, confirmed also by critical loads derived from Eq. (6):

$$p_{cr} = -6.7 \text{ kN/m} \quad (F13)$$

and

$$p_{cr} = -6.3 \text{ kN/m} \quad (F11)$$

Failure was due to crippling at mid-cross section, obviously due to post-critical buckling of the web with stresses distributed according to Fig. 5. This

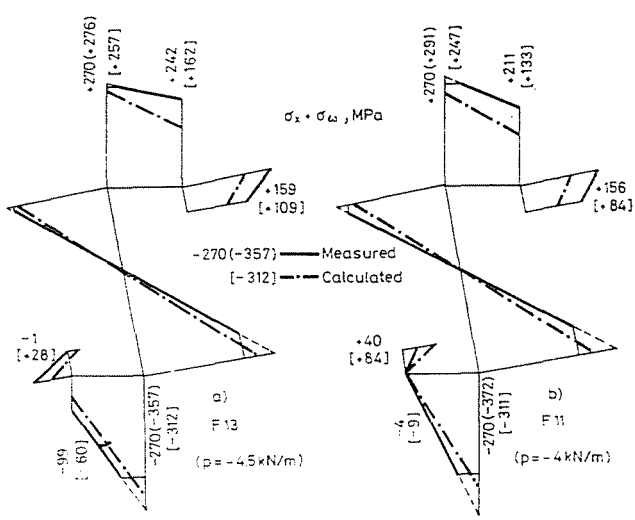

Fig. 5

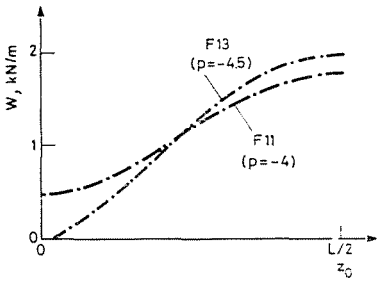

Fig. 6

fact argues for the use of a second-order spatial computation model where initial imperfections involve also the effect of residual manufacturing stresses (fictitious imperfection) in addition to manufacturing and montage imperfections. In this case — adequately assuming fictitious imperfections — beyond testing the first yield, the check of buckling of component plates is required. In our case, because of the width to thickness ratio of component plates of the tested section, this latter can be omitted if the post-critical reserve is irregarded.

Solving Eq. (6) by the finite difference method, taking initial imperfections of beam $F11$ into consideration, the load at normal stress

$$\sigma_x + \sigma_\omega = \sigma_F$$

obtained by iteration becomes:

$$p = -3.69 \text{ kN/m}.$$

Actual load capacity of the beam:

$$p_{\max} = -4.03 \text{ kN/m}.$$

Closeness of both values points to the calculation reliability.

Calculated value of the reaction force critical for the sheeting connections is seen in Fig. 6. In connection with the value for beam $F13$ it should be noted that at mid-beam, w has a value more than double that of:

$$p_x \frac{J_{xy}}{J_x}$$

In designing joints, in addition to shear stresses from w, also tensile stress from p_x has to be reckoned with.

Conclusions

Second-order analysis deduced for designing purlins made of cold-formed Z-sections fairly describes the actual behaviour of the beam. Calculated displacements and stresses are in fair agreement with results obtained on test beams simulating the effect of wind suction. Thereby this method may underly spatial model design of similar beams where the effect of residual stresses is reckoned with as fictitious inaccuracies. Properly selecting fictitious inaccuracy values, in the second-order analysis of the spatial model, check of plate buckling in addition to first yield suffices. No special difficulties arise in the application of the numerical method at the wanted accuracy.

Legend

A	cross-sectional area;
$^{\mathrm{I}}, ^{\mathrm{II}}, ^{\mathrm{III}}, ^{\mathrm{IV}}$	derivates with respect to z;
E	modulus of elasticity;
G	modulus of shear rigidity;
φ, φ_0	cross-sectional rotation;
J_x, J_y, J_{xy}	second moments of area about the centroidal coordinate axes;
$\bar{J}_y = J_y - J_{xy}^2/J_x$	
$D = J_x J_y - J_{xy}^2$	
J_{cs}	torsion constant;
J_ω	warping constant due to shear centre
$\bar{J}_\omega$	restrained axis of rotation
k	uniform restraint indicating the rate of elastic restraint by the sheeting;
m	distributed torque;
m_k	distributed torque due to the elastic restraint by the sheeting;
$M_{px}; M_u; M_v$	bending moments in planes y—z_0, v—z and u—z, resp.;
M_T	torque;
$\bar{\omega}$	sectorial coordinate of cross section points in rotation about an axis of restraint;
σ_x, σ_ω	normal stresses from bending and torsion, resp.;
$\sigma = \sigma_x + \sigma_\omega$	
p, p_x, p_y	uniformly distributed load and its components (kN/m);
r	radial distance of cross section points from the shear centre;
T_x, R_x	shear and reaction forces, resp.;
u, u_0, v	displacements of the beam centroid parallel, and normal, to the sheeting, resp.;

w	distributed reaction force corresponding to the supporting effect of the sheeting;
x, y, z_0	original coordinate system;
X, Y	coordinates of cross section points in an original centroidal coordinate system.

References

1. Experimental Testing of Purlins*. Research Report, Department of Steel Structures, Technical University, Budapest, 1983.
2. DOOLEY, J. F.: The Torsional Deformation of Columns of Monosymmetric I-section, with Restrained Axis of Twist, under Doubly Eccentric Load. Int. J. Mech. Sci., *9*. 585 (1967).
3. LINDNER, J.—KURTH, W.: Drehbettungswerte bei Unterwind. Bauingenieur *55*, 365 (1980).
4. KOLLBRUNNER, F.—BASLER, K.: Torsion. Springer, Berlin—Heidelberg, 1966.
5. DESIGN, Nodal Design and Control of Thin-Walled Steel Structures*. Technical Specifications ME-04 180—82.

Dr. Pál TOMKA H-1521 Budapest

* In Hungarian.